ROUGH-SEA DEGHOSTING OF SINGLE-SENSOR SEISMIC DATA USING THE KNOWLEDGE OF THE SEA SURFACE SHAPE

ENDRIAS G. ASGEDOM, OKWUDILI C. ORJI and WALTER SÖLLNER

PGS Geophysical AS, Oslo, Norway.
endrias.asgedom@pgs.com; okwudili.orji@pgs.com; walter.soellner@pgs.com

(Received September 23, 2016; revised version accepted January 7, 2017)

ABSTRACT

Asgedom, E.G., Orji, O.C. and Söllner, W., 2017. Rough-sea deghosting of single-sensor seismic data using the knowledge of the sea surface shape. *Journal of Seismic Exploration*, 26: 105-123.

Accurate receiver-side deghosting of marine seismic data can be performed for any sea surface condition when both pressure and vertical particle velocity information is available. However, conventional (hydrophone-only) marine acquisition delivers pressure-only data so additional information is required to perform proper deghosting. Here, we propose to use the shape of the sea surface above the receivers as additional information and formulate an inversion-based method to perform the deghosting. Deghosting pressure-only data from rough weather conditions using the inversion-based method is validated with both synthetic and field data examples. The effects of the sea surface roughness, the streamer depth and the noise in the input data are all analysed. Quantitative comparison of the inversion-based method with traditional flat sea surface deghosting shows the superiority of the inversion-based method for any sea surface condition.

KEY WORDS: rough sea surface, scattering, receiver-side deghosting, single-sensor deghosting, inversion, spectral division, marine seismic.

INTRODUCTION

Marine seismic data are encumbered with reflections of every event from the sea surface. Primary events interfere constructively or destructively with their sea surface counterparts (ghosts). This phenomenon penalizes the seismic resolution by limiting the effective bandwidth of the seismic data due to notches at particular frequencies that are related to the source and the receiver depths. Thus, marine seismic ghosts occur both on the source and the receiver sides. Removing the ghosts (deghosting) from marine seismic data can increase the usable frequency band by recovering the information at the ghost notch locations. Methods for removing ghost events can be acquisition or processing

0963-0651/17/$5.00

based. The methods can be optimized to specifically remove source-side or receiver-side ghosts. In processing based deghosting, the conventional pressure-only data are acquired and typically deghosted by spectral division using flat sea surface ghost function (Lindsey et al., 1960; Amundsen, 1993; Robinson and Treitel, 2008). Thus, this method ignores sea surface variation and therefore generally results in compromised time and depth images. Correct deghosting requires the measurement of pressure and normal component of the particle velocity data and then applying wavefield separation (Claerbout, 1976; Bar and Sanders, 1989; Carlson et al., 2007; Caprioli et al., 2012; Day et al., 2013).

In this work, we demonstrate that the knowledge of the sea surface shape is cardinal in deghosting any pressure-only data. In order to account for the roughness of the sea surface for deghosting pressure-only marine seismic data, continuous measurement of the sea surface heights are required. One possibility of obtaining the sea surface shape above the receivers is to directly measure the pressure fluctuation generated by the sea surface at the very low frequencies (Laws and Kragh, 2006). When such measurements are not available, we can utilize the recorded pressure-only data, from the active air gun sources, to infer the sea surface height above the receivers. For example, the sea surface height can be estimated from the notch distribution in the frequency-space domain (Grion et al., 2016) or we can extrapolate the total pressure wavefield to the sea surface and utilize the fact that the pressure is zero at the free surface (Asgedom et al., 2014b). Nevertheless, when both pressure and particle velocity recordings are available, the sea surface shape can be image after wavefield separation (Orji et al., 2010).

In order to account for the roughness of the sea surface for deghosting pressure-only marine seismic data, continuous measurement of the sea surface heights are required. The measured sea surface heights may be used to estimate the vertical particle velocity wavefields from the pressure data which then are used to perform wavefield separation (Robertsson and Kragh, 2002; Amundsen et al., 2005). In this paper, assuming the sea surface shape is known; we derive an integral inversion based deghosting method for pressure-only measurements. This new method incorporates the shape of the sea surface to model the down-going pressure wavefield recorded at the streamer level. This wavefield includes the scattered wavefield from the free surface and the direct down-going wavefield which are the prerequisite to deghosting the pressure-only measurement (Asgedom et al., 2014a; Asgedom et al., 2016).

In this work, we demonstrate that the knowledge of the sea surface shape is cardinal in deghosting any pressure-only data. For simplicity, we concentrate on receiver-side deghosting only. In order to study the effects of the degree of roughness of the sea surface shape may have on the deghosted data, both marginally rough and slightly rough sea states data, for a given streamer depth,

are deghosted using the new inversion-based technique. The analysis is repeated for different streamer depths for a given sea state and when the data is contaminated with noise. Furthermore, the deghosted results are compared to the flat sea surface deghosted counterparts. In all the analysed results, the inversion-based method outperforms the flat sea surface deghosting method. Moreover, the inversion-based method results in a pre-stack friendly receiver-side deghosted output. All the results are also validated using rough weather field data example.

METHOD

We consider a marine seismic data acquisition with sources at $\mathbf{r}_s = (\mathbf{x}_s, z_s)$ and receivers at $\mathbf{r}_r = (\mathbf{x}_r, z_r < z_s)$. Utilizing acoustic reciprocity of the time convolution type (Fokkema and van den Berg, 1993), we couple two states whose medium properties above the separation level $\mathbf{r}_{sep} = (\mathbf{x}_{sep}, z_r < z_{sep} < z_s)$ are identical (cf. Fig. 1). The first state, state A, is a physical state which resembles actual marine seismic acquisition. Here, pressure wavefields are generated at the sources and both the reflected wavefields at the subsurface and at the air water interface are recorded at the separation level. The second state, state B, is a hypothetical state which only contains air and water. In this state, state B, pressure wavefields are generated at the receiver locations using virtual sources and the results are measured at the separation level.

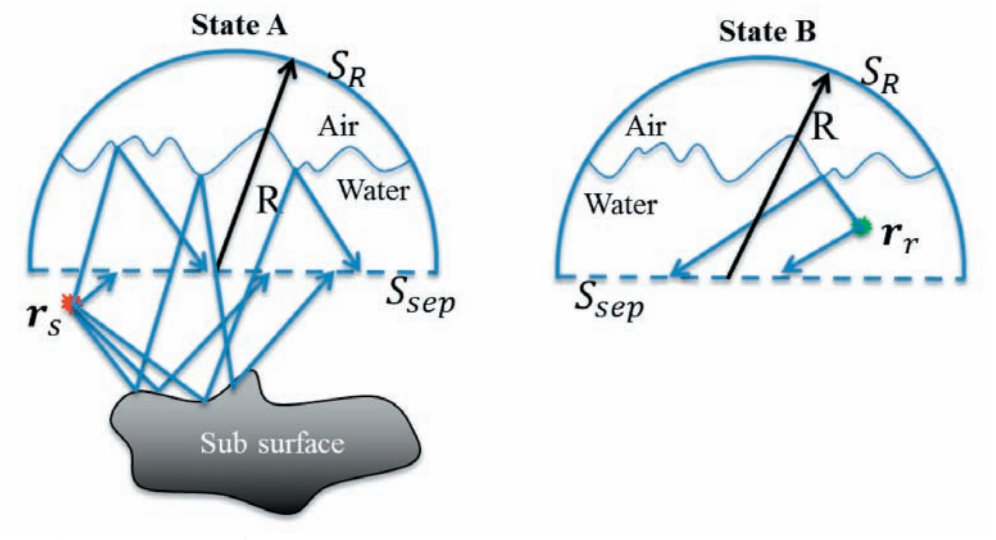

Fig. 1. The two states, A and B, coupled to generate a relationship between the total and up-going pressure wavefields. In this figure, the rays illustrate some of the possible ray paths that contribute to the measured wavefields at the separation level for each of the states.

In order to couple states A and B using acoustic reciprocity, we consider a volume enclosed by a hemispherical cup surface S_R with a radius of R and the separation level surface S_{sep}, so that $S = S_R + S_{sep}$. Assuming the radius goes to infinity and applying Sommerfeld's radiation condition over S_R, Rayleigh's acoustic reciprocity can be written as:

$$p^A(\omega,\mathbf{r}_r|\mathbf{r}_s)S^B(\omega) = -i\omega\rho \int_{S_{sep}} [p^B(\omega,\mathbf{r}_{sep}|\mathbf{r}_r)v_z^A(\omega,\mathbf{r}_{sep}|\mathbf{r}_s) - p^A(\omega,\mathbf{r}_{sep}|\mathbf{r}_s)v_z^B(\omega,\mathbf{r}_{sep}|\mathbf{r}_r)]\cdot\mathbf{n}dS_{sep} \quad , \qquad (1)$$

where p and $\mathbf{v}_z$ are the pressure and vertical component of the particle velocity, respectively. Moreover, $S^B(\omega)$, ρ and $\mathbf{n}$ are the virtual source signature in state B at an angular frequency ω, mass density and the unit normal vector at the surface S_{sep}, respectively. Decomposing the pressure and vertical component of the particle velocity into their up-going and down-going components; eq. (1) can be rewritten as (Wapenaar et al., 1990):

$$p^A(\omega,\mathbf{r}_r|\mathbf{r}_s)S^B(\omega) = -2i\omega\rho \int_{S_{sep}} [p^{B^+}(\omega,\mathbf{r}_{sep}|\mathbf{r}_r)v_z^{A^-}(\omega,\mathbf{r}_{sep}|\mathbf{r}_s) + p^{B^-}(\omega,\mathbf{r}_{sep}|\mathbf{r}_r)v_z^{A^+}(\omega,\mathbf{r}_{sep}|\mathbf{r}_s)]\cdot\mathbf{n}dS_{sep} \quad , \qquad (2)$$

with '$-$' and '$+$' denoting respectively up-going and down-going components of the wavefields. However, it is only the down-going wavefield contribution that is present in state B. Therefore, replacing $p^{B^-}(\omega,\mathbf{r}_{sep}|\mathbf{r}_r) = 0$ in Eq. (2), we obtain:

$$p^A(\omega,\mathbf{r}_r|\mathbf{r}_s)S^B(\omega) = -2i\omega\rho \int_{S_{sep}} [p^{B^+}(\omega,\mathbf{r}_{sep}|\mathbf{r}_r)v_z^{A^-}(\omega,\mathbf{r}_{sep}|\mathbf{r}_s)]\cdot\mathbf{n}dS_{sep} \quad , \qquad (3)$$

Eq. (3) describes the total pressure wavefield measured at the receiver location, generated by coupling the up-going vertical particle velocity wavefield in state A with the down-going pressure wavefield in state B. The integral relation in Eq. (3) can be written in a matrix form for a given frequency as:

$$\mathbf{p}^A\mathbf{S}^B = -2i\omega\rho\mathbf{P}^{B^+}\mathbf{V}_z^{A^-} \quad , \qquad (4)$$

with $\mathbf{P}^A \in \mathbb{C}^{n_r \times n_s}$, $\mathbf{P}^{B^+} \in \mathbb{C}^{n_r \times n_{sep}}$ and $\mathbf{V}_z^{A^-} \in \mathbb{C}^{n_{sep} \times n_s}$. Here, n_r, n_s and n_{sep} represent the number of receivers, sources and virtual receivers at the separation level, respectively. For any sea surface condition, eq. (4) can be used to solve for the up-going vertical particle velocity wavefield - provided that the total pressure wavefield is measured and the down-going pressure wavefield in state B is known. If information about the sea surface shape above each receiver is available, the down-going pressure wavefield in state B can be modeled (see

Appendix A). In addition, it is worth noting that $\mathbf{P}^{B+}$ may have notches which might create instability in the deghosting.

From the matrices in eq. (4), we can see that, the inversion for $\mathbf{V}_z^{A-}$ related to one source and one receiver position is a highly underdetermined problem. This can be constrained by including all source wavefields $\mathbf{P}^{B+}$ (ideally, the number of virtual source wavefields should be equal to the number of receivers on the separation level) related to one common source gather of the input data $\mathbf{P}^{A}$. Hence, the common source gather is the natural domain for receiver deghosting by inversion of eq. (4).

Selecting the separation level to be flat, we can convert the up-going vertical particle velocity into up-going pressure using (Amundsen, 1993)

$$P^{A-}(\omega,\mathbf{k}_{sep},z_{sep}|\mathbf{r}_s) = (\omega\rho/k_z)V_z^{A-}(\omega,\mathbf{k}_{sep},z_{sep}|\mathbf{r}_s) \quad , \tag{5}$$

where $\mathbf{k}_{sep}$ is a lateral wavenumber vector at the separation level, z_{sep} is the depth of the separation level and k_z is the vertical wavenumber. P^{A-} and V_z^{A-} denote, respectively, the pressure and vertical velocity wavefields in frequency wavenumber domain.

When there is no information available about the sea surface, we often assume it is flat and set a reflection coefficient of -1. Utilizing the analytic form of the Green's function in a homogenous medium with a free surface boundary condition, and considering translational shift invariance of the virtual source wavefields p^{B+} with $z_{sep} = z_r$, the matrix equation in eq. (4) reduces to spectral multiplication (cf. Appendix B) (Fokkema and van den Berg, 1993; Amundsen, 2001)

$$P^{A}(\omega,\mathbf{k}_r,z_r|\mathbf{x}_s,z_s) = G_p^{flat}(\omega,\mathbf{k}_r)P^{A-}(\omega,\mathbf{k}_r,z_r|\mathbf{x}_s,z_s) \quad , \tag{6}$$

where $G_p^{flat}(\omega,\mathbf{k}_r) = 1 - \exp(2ik_zz_r)$ is the flat sea surface ghost function and $\mathbf{k}_r$ is the lateral wavenumber vector. Moreover, k_z is the vertical wavenumber and it is defined as

$$k_z = \begin{cases} \{(\omega/V)^2 - \mathbf{k}_r^2\}^{1/2} \, , & \text{when } |\mathbf{k}_r| \leq |\omega/V| \\ i\{\mathbf{k}_r^2 - (\omega/V)^2\}^{1/2} \, , & \text{when } |\mathbf{k}_r| > |\omega/V| \end{cases} \quad , \tag{7}$$

where V is the speed of seismic wave in water. In all the analysis in this paper, we consider the evanescent wave contribution is small and thus the energy of the recorded data outside the signal cone (i.e., $|\mathbf{k}_r| > |\omega/V|$) is filtered out. In addition, to avoid the evanescent wave contribution from the modelled $\mathbf{P}^{B+}$ in eq. (4), we placed the separation level (i.e., where we have virtual receivers) away from the receiver location (i.e., where we have virtual sources).

SYNTHETIC DATA EXAMPLES

In this section we utilize synthetically modelled data to investigate the effects of static rough sea surfaces in single sensor (i.e., hydrophone-only) deghosting methods. The data modelling assumes the sea surface is static and the medium between the streamer and the sea surface is homogenous.

Synthetic data was computed from a model consisting of a static rough sea surface and a flat sea floor reflector (cf. Fig. 2). The data computation configuration consists of a source and receivers at a depth of 5 m and 20 m, respectively. The streamer is 3000 m long and the receivers are spaced 3 m. The separation level, needed to perform the inversion-based deghosting, is selected to be 5 m below the streamer depth level. Two test cases representing two sea surface conditions were considered, - the marginally rough and slightly rough sea states.

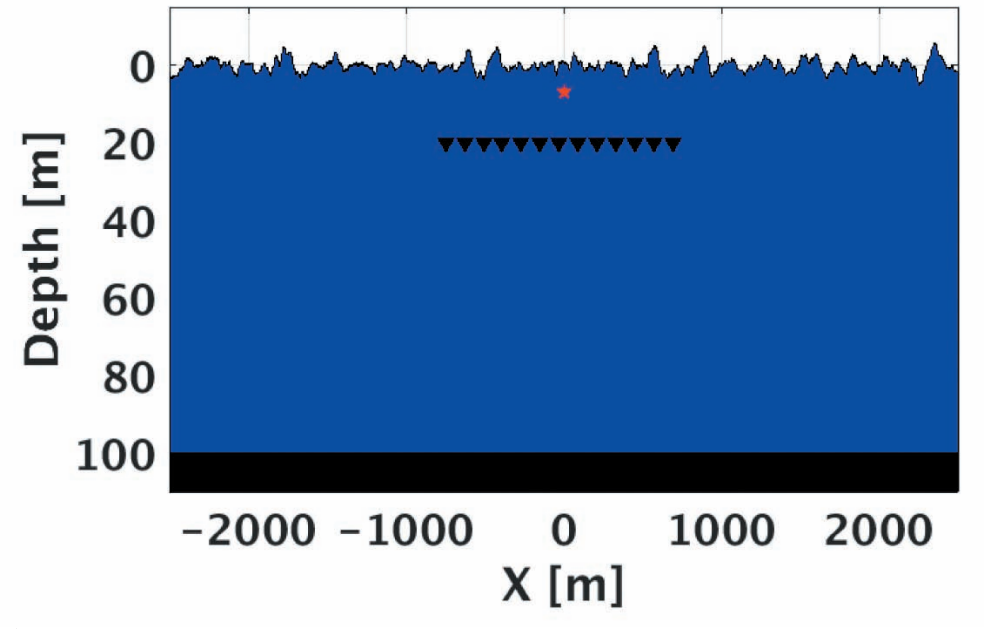

Fig. 2. Synthetic data computation geometry.

The total pressure in state A (i.e., the data we aim to deghost) and the down-going pressure in state B (i.e., the data containing all the information about the sea surface), were both modelled from the two sea surface conditions. The two sea surface conditions are characterized by the SWH (Significant Wave Height). The marginally rough sea condition has SWH of 6.6 m while the slightly rough sea has a SWH of 1.36 m. Figs. 3a - 3d show the total pressure from the two sea surfaces in TX (time-space) and FK (frequency-wavenumber)

domains. In the TX plots, the main up-going event is shown in blue with the bubble part of the source wavelet shown in different shades of brown and black whereas the main down-going event is shown in red. The undulations visible in the down-going part of the total pressure are stronger in the marginally rough sea surface condition data (cf. Fig. 3a) compared to that of the calmer sea surface condition (cf. Fig. 3b). In the FK plots, the effect of the down-going wavefield scattering from a rough sea surface is manifested as notch diversity (i.e., superposition of different notch frequencies). The notch diversity is proportional to the sea surface roughness (cf. Figs. 3d and 3e). Observe that the modelled up-going pressure field contains only the subsurface reflection and thus, is smooth in both TX and FK domains (cf. Figs. 3c and 3f)

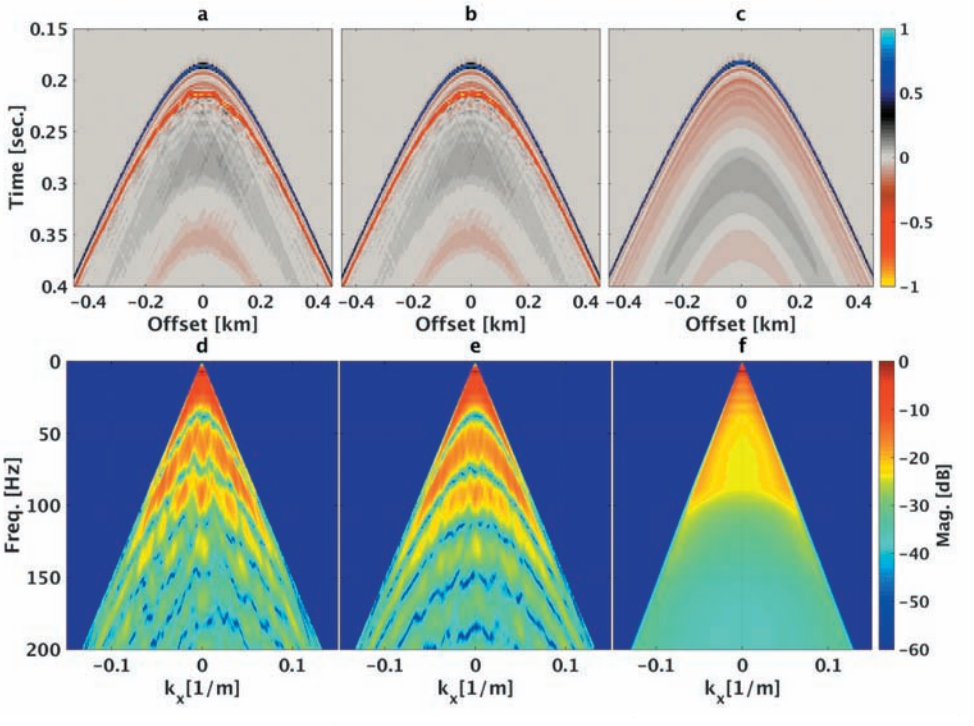

Fig. 3 Modelled total pressure from marginally rough (a) and slightly rough (b) sea surfaces and the up-going pressure wavefield (c) in TX domain. The amplitude spectra in FK of the total pressure from marginally rough (d) and slightly rough (e) sea surfaces and the up-going wavefield (f).

We now apply the inversion based deghosting eq. (4) and the conventional flat sea surface deghosting eq. (6) to obtain up-going pressure wavefields. In order to stabilize the deghosting process at the notch locations (for the flat sea

deghosting) and the conversion of up-going vertical particle velocity into the up-going pressure (i.e., when k_z is zero at 90° emergence angle), we dampened the input data with a small exponential factor and added the same factor as an imaginary number in the temporal frequency axis of the operators. Finally, the exponential dampening was removed from the output data to ensure the wavefields are preserved. Note that when applying the inversion-based deghosting using eq. (4), no stabilization was included at the notch frequencies.

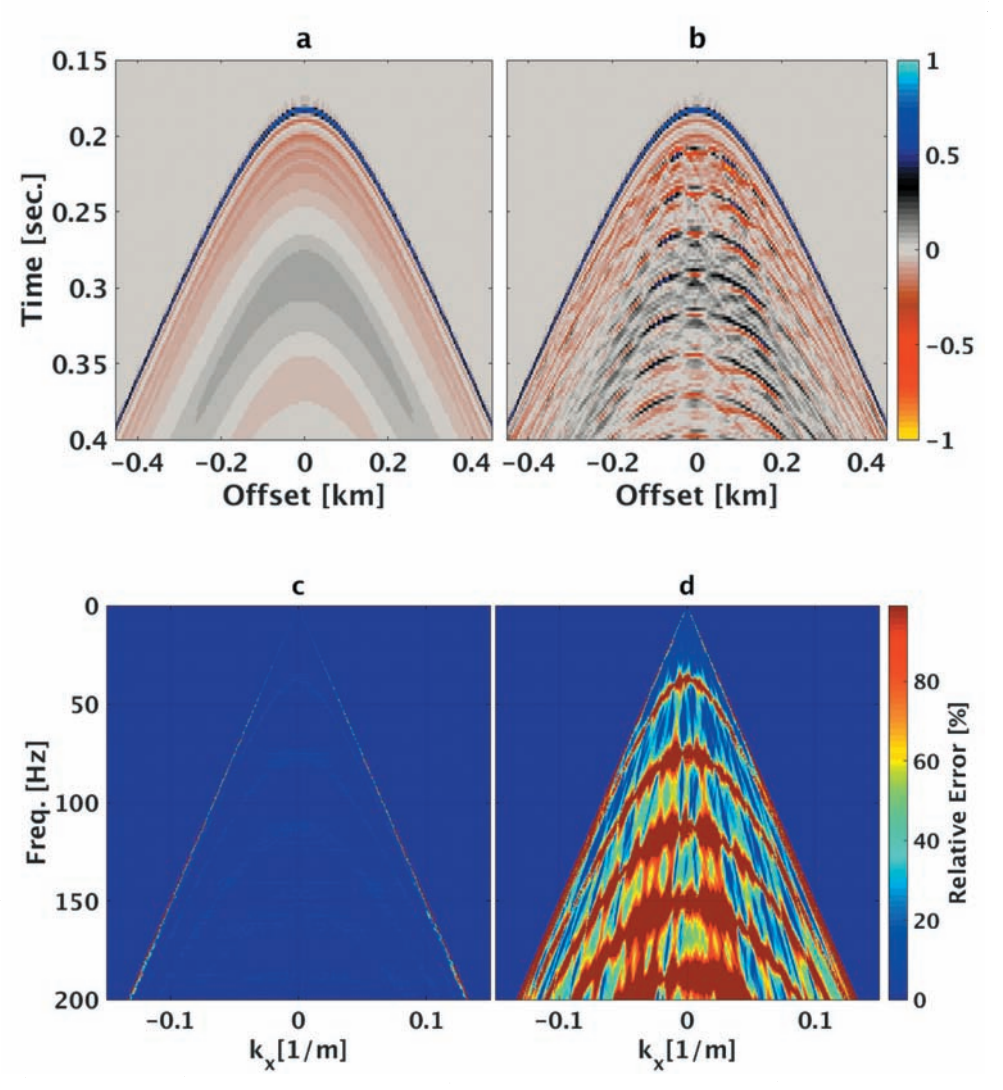

Fig. 4 Marginally rough sea surface deghosting results for a streamer depth of 20 m in TX for inversion-based (a) and deghosting using flat sea surface assumption (b). The percentage relative error for the inversion-based (c) and flat sea surface deghosting (d).

After applying inversion-based deghosting, the resulting up-going vertical particle velocity wavefield was converted into the up-going pressure using eq. (5). Fig. 4a shows the result for the marginally rough sea surface case. This result shows an excellent match with the modelled up-going pressure of Fig. 3c. On the contrary, for the deghosting using flat sea surface assumption the result shown in Fig. 4b has residual down-going energy and a ringing feature. To quantify the differences between the modelled and the deghosted results, we

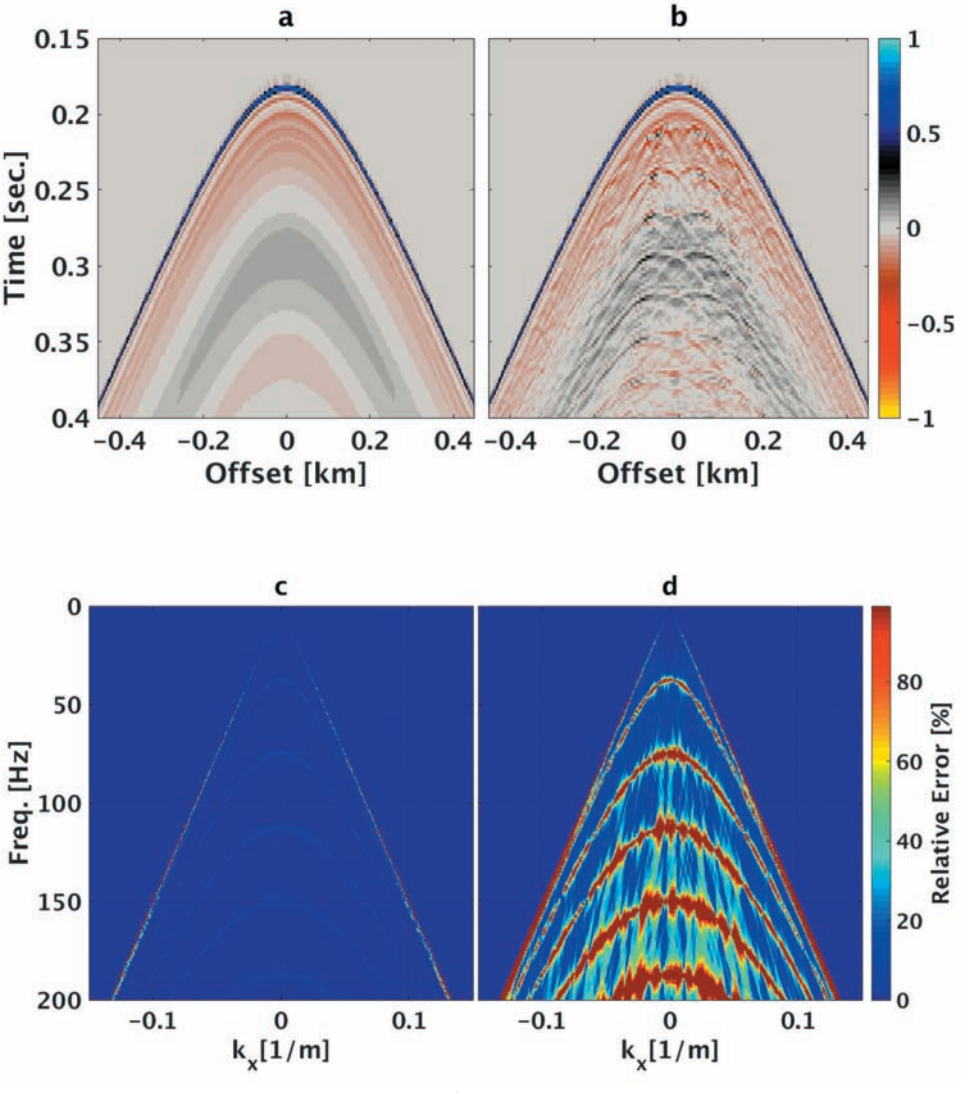

Fig. 5. Slightly rough sea surface deghosting results for a streamer depth of 20 m in TX for inversion-based (a) and flat sea surface assumption deghosting (b). The percentage relative error for the inversion-based (c) and flat sea surface deghosting (d).

computed the percentage relative error in FK domain. Fig. 4c shows the percentage relative error from the inversion-based deghosting, where only very small errors close to the notch locations can be observed. However, the errors of the deghosting based on flat sea surface assumption shown in Fig. 4d are relatively high as a result of wrong prediction of the notch locations and also wrong estimation of the scattered wavefield from the sea surface.

The same analysis is performed for the slightly rough sea surface case. Figs. 5a - 5d show the inversion-based and flat sea surface assumption based deghosting results. The relative error of the inversion-based deghosting still shows very small but more localized errors that are only slightly larger in comparison to the result of the marginally rough sea surface case (compare Figs. 4c and 5c). This is because the notch diversity in the down-going pressure in state B, $\mathbf{P}^{B+}$ reduces as the roughness of the sea surface reduces thus making the inversion-based deghosting increasingly unstable at the notch frequencies. In the slightly rough sea surface data that is deghosted with flat sea assumption, the error in the region between the notch frequencies is smaller in comparison to the marginally rough sea surface counterpart.

The experiment for the slightly rough sea surface case was repeated but now with the streamer moved up to 10 m depth. The results of the inversion-based and flat sea surface assumption based deghosting are shown in Figs. 6a - 6d. In comparison to the 20 m streamer depth inversion-based deghosting counterpart, the 10 m streamer inversion-based deghosting notch related errors are still small but now spectrally spread over larger regions. On the other hand, the slight difference in the errors is because the effect of the sea surface roughness in the acquired seismic data is determined by the depth of the receivers (i.e., the scattered wavefield is healing with increasing propagation distance from the scatter point). Moreover, observe that the deghosting based on flat sea surface assumption has larger relative errors compared to the case of the 20 m streamer depth.

The inversion-based deghosting algorithm has been shown to give excellent results in comparison to the deghosting based on flat sea surface assumption. In reality, field data are contaminated by noise. Thus, in order to illustrate the effects of noise on the robustness of the algorithm, we added Gaussian random noise to the input total pressure data from the slightly rough surface with streamer located at 10 m depth. Fig. 7a shows the amplitude spectra, at vertical emergence angle, of the noise free total pressure field and the additive noise. Observe that there is generally poor signal-to-noise ratio around the notch frequencies in comparison to the other parts of the spectrum of total pressure field. The inversion-based deghosting and flat sea surface deghosting were then both applied, and the results are shown in Figs. 7b and 7c. The results (amplitude spectra, at vertical emergence angle) of the inversion-based deghosting shown in Fig. 7b for the noise free and the data with

additive noise demonstrate that the algorithm is sensitive to noise, especially at the notch locations. Nevertheless, unlike the flat sea surface deghosting results shown in Fig. 7c, the inversion-based method provides the correct up-going pressure wavefield at locations away from the notch frequencies. Notwithstanding, it is pertinent to note that signal-to-noise ratio at higher frequency notch locations of field data are significantly higher in contrast to that used in the synthetic data example.

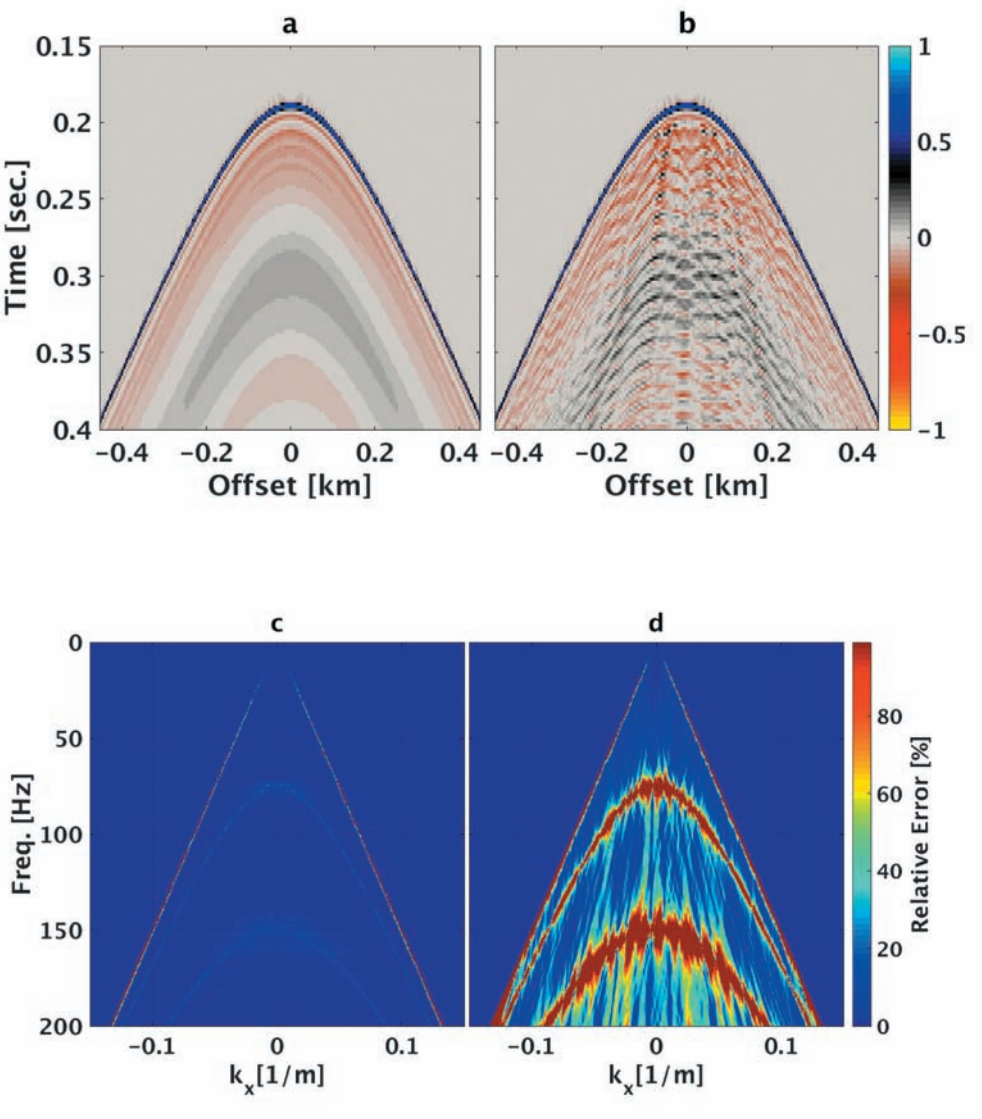

Fig. 6 Slightly rough sea surface deghosting results for a streamer depth of 10 m in TX for inversion-based (a) and flat sea surface assumption deghosting (b). The percentage relative error for the inversion-based (c) and flat sea surface deghosting (d).

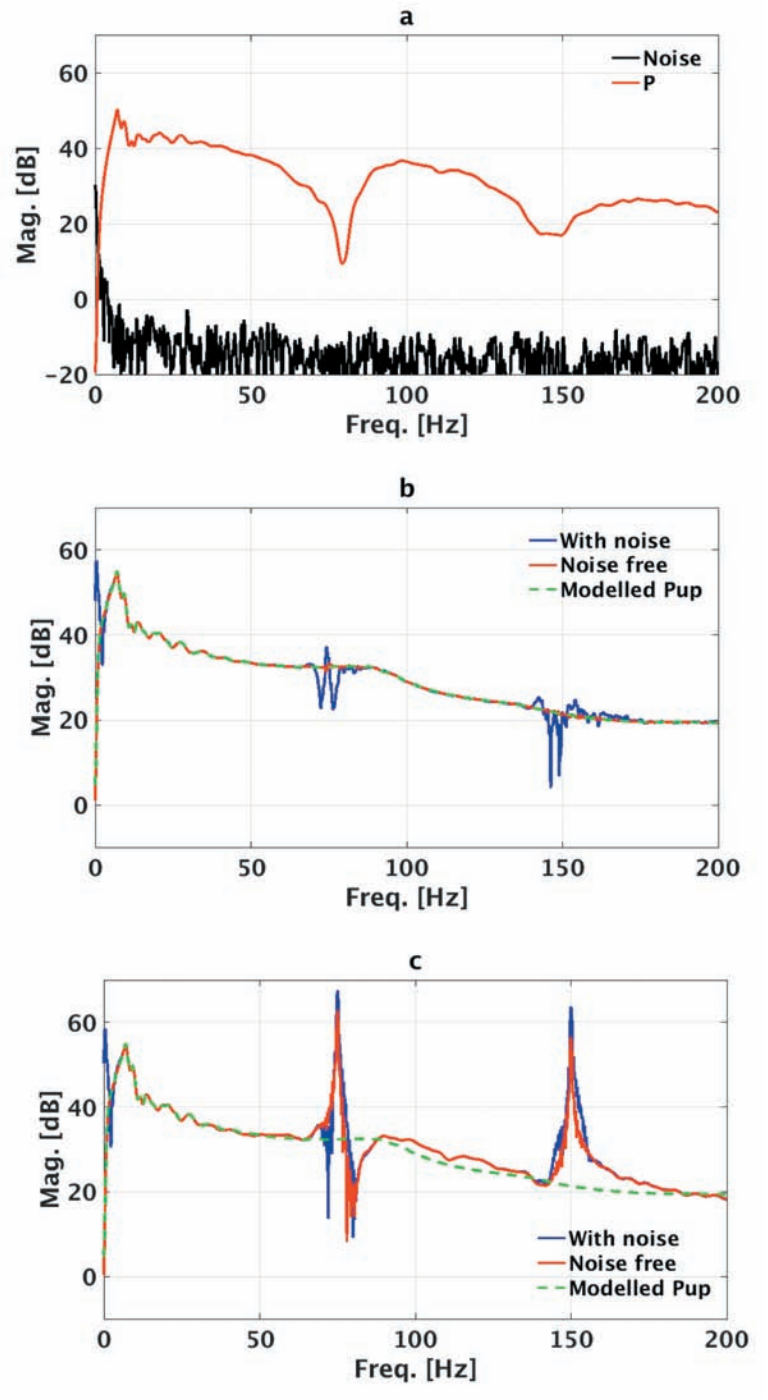

Fig. 7. Amplitude spectra at vertical emergence angle of: the noise free total pressure and the additive noise (a), after the inversion-based deghosting of the input data with and without additive noise (b), and after flat sea surface deghosting of the input data with and without additive noise (c).

FIELD DATA EXAMPLES

Except for experimental purposes, field data acquired under marginally rough sea conditions are rare because of operational hazards. Thus, a field data set acquired during a moderately rough weather condition is used to validate the observations in the synthetic data examples. The data was acquired using dual-sensor streamer which allows correct separation of the total pressure wavefield into the up-going and down-going components. The total pressure for a selected shot gather is shown in TX and FK domains in Figs. 8a and 8b, respectively. The FK spectrum is computed within the selected window shown in Fig. 8a. The presence of rough sea surface during the data acquisition manifests itself in the total pressure data as the undulations of the down-going part of the data in TX and diversity of notches in the FK domain.

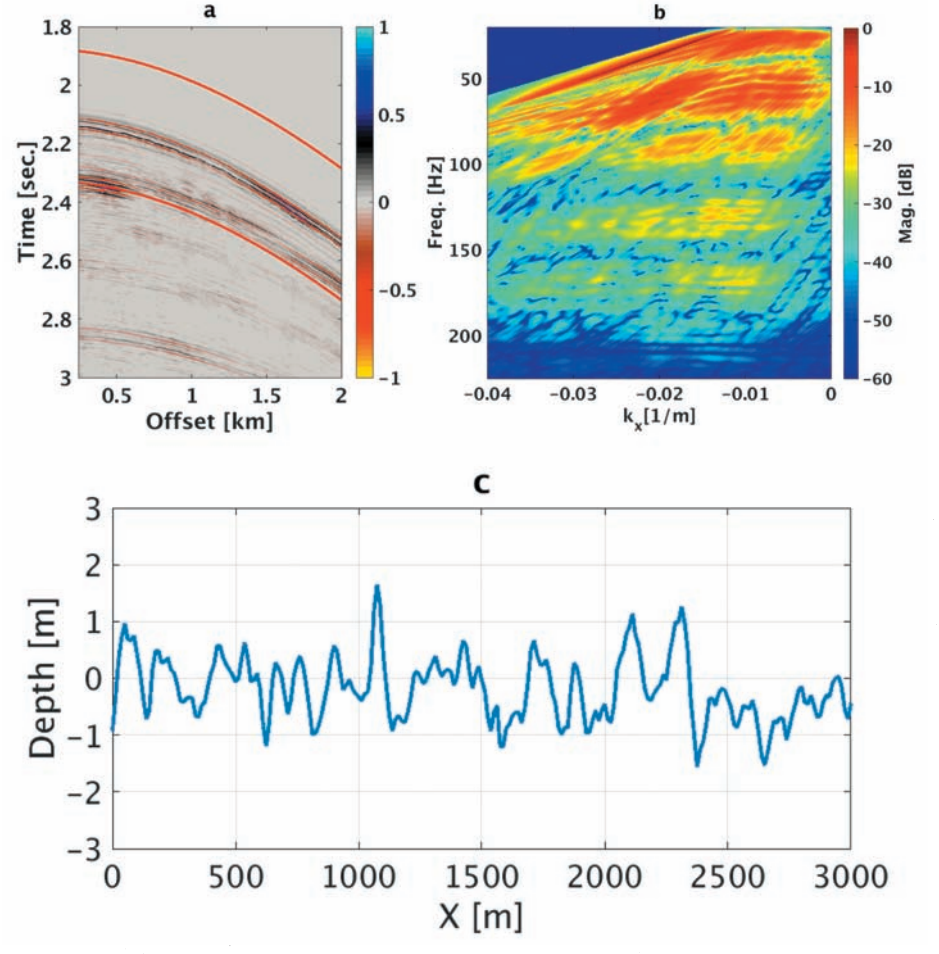

Fig. 8. The total pressure in TX (a) and the corresponding FK within the window shown in (a) and (b). The imaged sea surface within the same window (c).

In order to apply the inversion-based deghosting, the knowledge of the sea surface shape is required. Firstly, the image of the sea surface above the receivers is obtained by extrapolating the higher frequencies (i.e., above 20 Hz) of the separated up-going and down-going pressure wavefields (e.g., Orji et al., 2010). The resulting imaged sea surface is shown in Fig. 8c. The computed SWH of the imaged sea surface correlates well with the reported SWH in the observer's log (approximately 3 m). The next step in the inversion-based deghosting is to compute the down-going pressure wavefield in state B (cf. Fig.1). Here, we consider state B contains homogenous water and air medium and we utilized a 2D Green's function to perform the modelling based on eq. (A-1). Subsequently, we applied the inversion-based deghosting from eq. (4) to obtain the up-going vertical particle velocity wavefield which is then converted into up-going pressure wavefield using eq. (5). In addition, the deghosting based

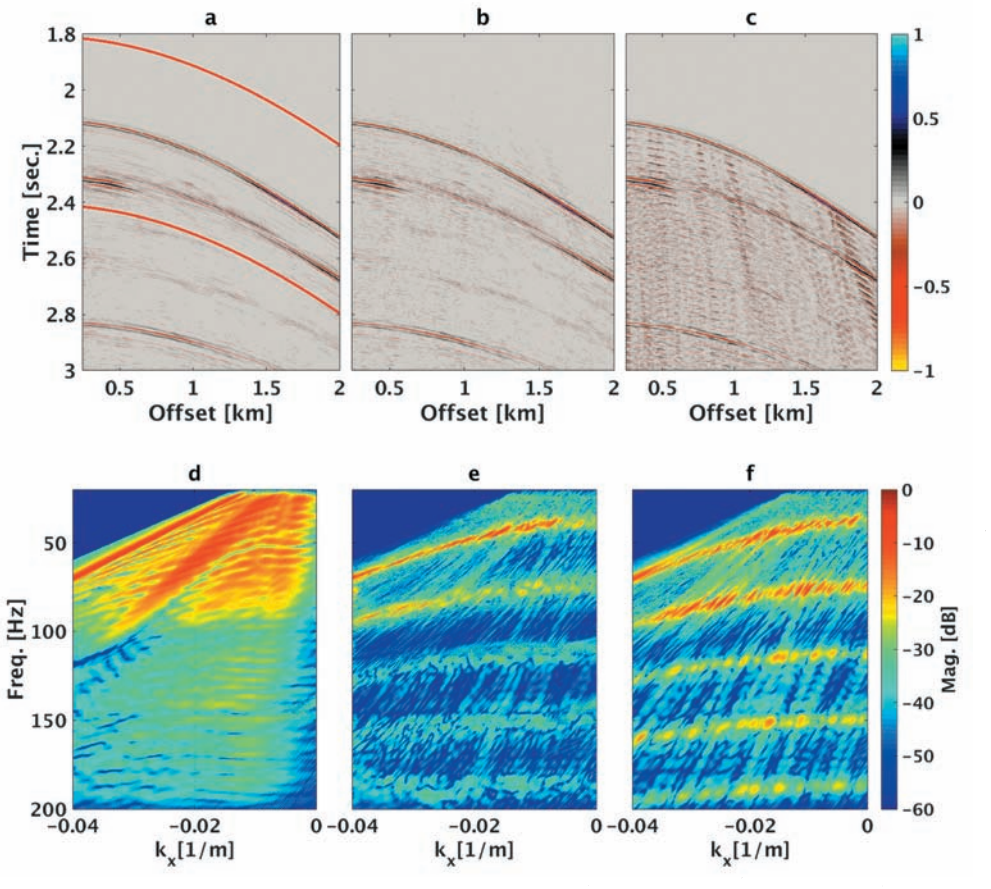

Fig. 9. TX plots of the wavefield separated up-going wavefield (a); inversion-based deghosted up-going wavefield (b) and flat sea surface deghosting result (c). The FK plots of the wavefield separated up-going wavefield (d), the residual of the inversion-based deghosting (e), and the residual of the flat sea surface assumption (f).

on flat sea surface assumption was also applied using eq. (6). The results are shown in Figs. 9b (inversion-based) and 9c (flat sea surface deghosting). As expected and similar to the synthetic data results, the deghosting based on flat sea surface assumption is dominated by residual down-going energy and ringing features while the inversion-based result closely resembles the up-going wavefield obtained from wavefield separation (cf. Figs. 9a and 9d) albeit some instability artifacts around the nominal notch locations.

To analyse the performance of the inversion-based and the flat sea surface assumption based deghosting methods, we compared the results with the wavefield separated up-going wavefield for the frequencies above 20 Hz. The difference between the two deghosting methods and the reference (i.e., the up-going wavefield result from dual sensor measurements) is shown in FK domain in Figs. 9e and 9f. The residual due to the inversion-based deghosting shows in general smaller errors between the notch frequencies and is more stable at higher frequency notches. However, since the imaged sea surface may differ from the actual sea surface in the field data, (for example due to aliasing and lack of very high frequencies in the data), the down-going pressure wavefield in state B required to perform the inversion-based deghosting might contain inaccuracies in the predicted scattered wavefields from the sea surface. This could explain the small residual observed between the inversion-based algorithm and the wavefield separated up-going wavefield in the areas between the notch locations. This is in contrast to the flat sea deghosting algorithm which shows larger errors at all frequencies.

CONCLUSION

Correct wavefield separation into up-going and down-going wavefields requires the knowledge of both total pressure and total vertical particle velocity at the streamer level. If only one wavefield is measured, one needs to provide additional knowledge of the sea surface shape. In this paper, we showed how to perform a proper receiver-side deghosting when the available information is the total pressure wavefield at the streamer level and the sea surface shape above each of the receivers. This deghosting method provides reliable up-going wavefields for rough sea surfaces if the signal-to-noise ratio is sufficiently high. However, when the signal-to-noise ratio is poor, the deghosting method might fail and amplify a significant amount of noise especially around the lower frequency notches.

ACKNOWLEDGEMENTS

The authors thank PGS for the permission to publish this work, and Jon Sheiman for the constructive comments that helped to improve the paper.

REFERENCES

Amundsen, L., 1993. Wavenumber-based filtering of marine point-source data. Geophysics, 58: 1335-1348.

Amundsen, L., 2001. Elimination of free-surface related multiples without need of the source wavelet. Geophysics, 66: 327-341.

Amundsen, L., Røsten, T., Robertsson, J.O.A. and Kragh, E., 2005. Rough-sea deghosting of streamer seismic data using pressure gradient approximations. Geophysics, 70: v1-v9.

Asgedom, E.G., Orji, O.C. and Söllner, W., 2014a. Pressure normal derivative extraction for arbitrarily shaped surfaces. Expanded Abstr., 84th Ann. Internat. SEG Mtg., Denver: 4243-4247.

Asgedom, E.G., Orji, O.C. and Söllner, W. 2014b. Methods and systems to separate wavefields using pressure wavefield data. Patent application number: US 2015/0301210 A1. Filed 10.23.2014

Asgedom, E.G., Orji, O.C., Klüver, T., Tabti, H. and Söllner, W., 2016. On broadband data and rough sea surface receiver deghosting. Extended Abstr., 78th EAGE Conf., Vienna: Tu SRS3 03

Bar, F.J. and Sanders, J.I., 1989. Dual-sensor summation of noisy ocean-bottom data. Expanded Abstr., 59th Ann. Internat. SEG Mtg., Dallas: 653-656.

Caprioli, P., Ízdemir, K., van Manen, D.J., Mahat, S., Ízbek, A., Kragh, E. and Christie, P., 2012. Combination of multi-component streamer pressure and vertical particle velocity - Theory and application to data. Expanded Abstr., 82nd Ann. Internat. SEG Mtg., Las Vegas: 1-5.

Carlson, D., Long, A., Söllner, W., Tabti, H., Tenghamn, R. and Lunde, N., 2007. Increased resolution and penetration from a towed dual-sensor streamer. First Break, 25: 71-77.

Claerbout, J.F., 1976. Fundamentals of Geophysical Data Processing. McGraw-Hill, Inc., New York.

Day, A., Klüver, T., Söllner, W., Tabti, H. and Carlson, D. 2013. Wavefield-separation methods for dual-sensor towed-streamer data. Geophysics, 78: WA55-WA70.

Fokkema, J.T. and van den Berg, P.M. 1993. Seismic applications of acoustic reciprocity. Elsevier Science Publishers, Amsterdam.

Grion, S., Telling, R. and Holland, S., 2016. Rough sea estimation for phase-shift de-ghosting. Expanded Abstr., 86th Ann. Internat. SEG Mtg., Dallas: 5129-5133.

Laws, R. and Kragh, E., 2006. Sea surface shape derivation above the seismic streamer. Geophys. Prosp., 54: 817-828.

Lindsey, J.P., 1960. Elimination of seismic ghost reflections by means of a linear filter. Geophysics, 25: 130-140.

Orji, O.C., Söllner, W. and Gelius, L.J., 2010. Imaging the sea surface using a dual-sensor towed streamer. Geophysics, 75: V111-V118.

Orji, O.C., Söllner, W. and Gelius, L.J., 2011. Effects of time-varying sea surface in marine seismic data. Geophysics, 77: 33-43.

Robinson, E.A. and Treitel, S., 2008. Digital Imaging and Deconvolution: The ABCs of Seismic Exploration and Processing. SEG, Tulsa, OK.

Robertsson, J.O.A. and Kragh, E., 2002. Rough-sea deghosting using a single streamer and a pressure gradient approximation. Geophysics, 67: 2005-2011.

Thorsos, E., 1988. The validity of the Kirchhoff approximation for rough surface scattering using a Gaussian roughness spectrum. J. Acoust. Soc. Am., 83: 78-92.

Wapenaar, C.P.A., Herrmann, P., Verschuur, D.J. and Berkhout, A.J., 1990. Decomposition of multicomponent seismic data into primary P- and S-wave responses. Geophys. Prosp., 38: 633-661.

APPENDIX A

To derive the relation used for computing the down-going pressure wavefield in state B, we consider acoustic reciprocity of the time convolution type (Fokkema and van den Berg, 1993), where the pressure wavefield in state B can be generated as a result of coupling of two states (cf. Fig. A-1). In the first state, state C, we generate a pressure wavefield with a source wavelet $s^C(\omega) = s^B(\omega)$ and record the data at the free surface $\mathbf{r}_{fs}$. In the second state, state D, which is a homogeneous medium without any physical boundary, we generate pressure wavefield with an impulsive source (i.e., with Dirac source wavelet) and record the data at the free surface.

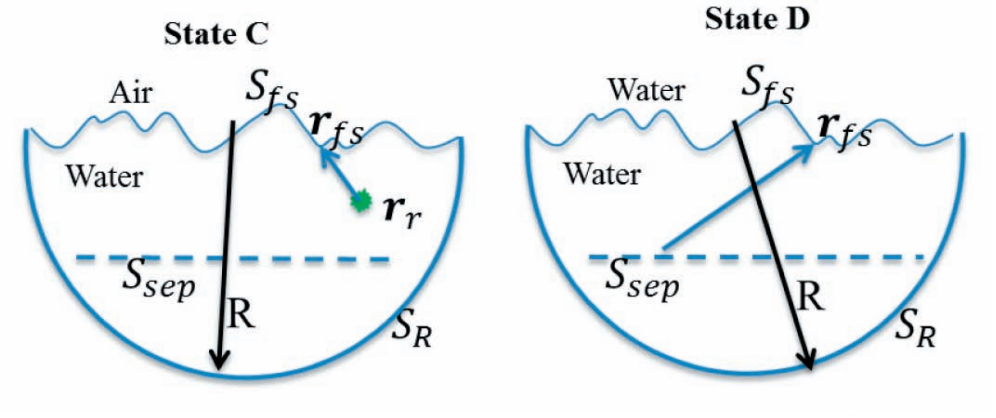

Fig. A-1. The two states, C and D, needed for generating the down-going pressure wavefield in state B.

Using the fact that the pressure field in state C at the free surface is zero (i.e., in state C the free surface is a physical boundary), the resulting acoustic reciprocity relation can be written as

$$p^{B+}(\omega,\mathbf{r}_{sep}|\mathbf{r}_r) = p^D(\omega,\mathbf{r}_r|\mathbf{r}_{sep})S^B(\omega) - \int_{S_{fs}} \{p^D(\omega,\mathbf{r}_{fs}|\mathbf{r}_{sep})[\partial p^C(\omega,\mathbf{r}_{fs}|\mathbf{r}_r)/\partial \mathbf{n}_{fs}]\} dS_{fs} \quad , \qquad \text{(A-1)}$$

where $\mathbf{n}_{fs}$ is the normal at the free surface. The first and second terms in the right hand side of eq. (A-1) represent the direct and scattered wavefields, respectively. To compute the down-going pressure wavefield in state B using eq. (A-1), the normal derivative of the pressure field at the sea surface in state C is first computed. This can be achieved either using Kirchhoff approximation or applying integral inversion (Torsos, 1988; Orji et al., 2011).

APPENDIX B

In this Appendix we derive the relationship between the total pressure P^A and the up-going pressure P^{A^-} and show, if the sea surface is assumed flat, this leads to the well-known deghosting relation in frequency wavenumber domain. We start from eq. (3) and apply lateral translation invariance condition on P^{B^+} (i.e., adding a lateral shift of $\mathbf{x}_s - \mathbf{x}_{sep}$ on both source and receiver coordinates)

$$p^{B^+}(\omega,\mathbf{r}_{sep}\,|\,\mathbf{r}_r) \equiv p^{B^+}(\omega,\{\mathbf{x}_{sep},z_{sep}\}\,|\,\{\mathbf{x}_r,z_r\}) =$$

$$p^{B^+}(\omega,\{\mathbf{x}_s,z_{sep}\}\,|\,\{\mathbf{x}_r + \mathbf{x}_s - \mathbf{x}_{sep},z_r\}) \quad . \tag{B-1}$$

Next, replacing eq. (B-1) into eq. (3)

$$p^A(\omega,\{\mathbf{x}_r,z_r\}\,|\,\{\mathbf{x}_s,z_s\})s^B(\omega)$$

$$= -2i\omega\rho \int_{S_{sep}} [p^{B^+}(\omega,\{\mathbf{x}_s,z_{sep}\}\,|\,\{\mathbf{x}_r + \mathbf{x}_s - \mathbf{x}_{sep},z_r\})$$

$$\times\, v_z^{A^-}(\omega,\{\mathbf{x}_{sep},z_{sep}\}\,|\,\{\mathbf{x}_s,z_s\})]d\mathbf{x}_{sep} \quad . \tag{B-2}$$

Utilizing Parseval's identity, eq. (B-2) can be written as

$$p^A(\omega,\{\mathbf{x}_r,z_r\}\,|\,\{\mathbf{x}_s,z_s\})s^B(\omega)$$

$$= [-2i\omega\rho/(2\pi)^2] \int_{-\infty}^{\infty} [p^{B^+}(\omega,\{\mathbf{x}_s,z_{sep}\}\,|\,\{\mathbf{k}_{sep},z_r\})$$

$$\times\, v_z^{A^-}(\omega,\{\mathbf{k}_{sep},z_{sep}\}\,|\,\{\mathbf{x}_s,z_s\})]\exp[i\mathbf{k}_{sep},(\mathbf{x}_r + \mathbf{x}_s)]d\mathbf{k}_{sep} \quad , \tag{B-3}$$

where $\mathbf{k}_{sep}$ is the lateral wavenumber vector in the direction of the separation level.

Taking the spatial Fourier transform of eq. (B-3) in the receiver direction, we obtain

$$p^A(\omega,\{\mathbf{k}_r,z_r\}\,|\,\{\mathbf{x}_s,z_s\})s^B(\omega)$$

$$= -2i\omega\rho \int_{-\infty}^{\infty} [p^{B^+}(\omega,\{\mathbf{x}_s,z_{sep}\}\,|\,\{\mathbf{k}_{sep},z_r\})$$

$$\times\, v_z^{A^-}(\omega,\{\mathbf{k}_{sep},z_{sep}\}\,|\,\{\mathbf{x}_s,z_s\})\exp(i\mathbf{k}_{sep},\mathbf{x}_s)]d\mathbf{k}_{sep}$$

$$\times\, [1/(2\pi)^2] \int_{-\infty}^{\infty} \exp[i(\mathbf{k}_{sep} - \mathbf{k}_r),\mathbf{x}_r]d\mathbf{x}_r \quad . \tag{B-4}$$

Utilizing the property of a Dirac function and the relation between P^{A^-} and $V_z^{A^-}$ in eq. (5), we can express eq. (B-4) as

$$p^A(\omega,\{\mathbf{k}_r,z_r\}\,|\,\{\mathbf{x}_s,z_s\})s^B(\omega)$$

$$= -2ik_z p^{B^+}(\omega,\{\mathbf{x}_s,z_{sep}\}\,|\,\{\mathbf{k}_r,z_r\})$$

$$\times\ p^{A^-}(\omega,\{\mathbf{k}_r,z_{sep}\}\,|\,\{\mathbf{x}_s,z_s\})\exp(i\mathbf{k}_r,\mathbf{x}_s)\quad . \tag{B-5}$$

For a flat sea surface with a reflection coefficient of -1 and assuming the medium between the separation level and the sea surface is homogenous, we can express p^{B^+} for a Dirac source [i.e., $s^B(\omega) = 1$] as (Amundsen, 2001)

$$p^{B^+}(\omega,\{\mathbf{x}_s,z_{sep}\}\,|\,\{\mathbf{k}_r,z_r\})$$

$$= [\{\exp(ik_z|z_{sep} - z_r|)$$

$$- \exp(ik_z|z_{sep} + z_r|)\}\exp(-ik_r\mathbf{x}_s)]/-2ik_z\quad , \tag{B-6}$$

where k_z is the vertical wavenumber for the wavenumber in the receiver direction. Finally, replacing eq. (B-6) into eq. (B-5) and taking $z_{sep} = z_r$

$$p^A(\omega,\{\mathbf{k}_r,z_r\}\,|\,\{\mathbf{x}_s,z_s\})s^B(\omega)$$

$$= \{1 - \exp(2ik_z z_r)\}p^{A^-}(\omega,\{\mathbf{k}_r,z_{sep}\}\,|\,\{\mathbf{x}_s,z_s\})\quad . \tag{B-7}$$